Lasers in Manufacturing and Materials Processing (2024) 11:661–676
https://doi.org/10.1007/s40516-024-00263-8

RESEARCH

Probing the Role of Temperature-Dependent Material Property Profiles During Laser Forming Via Finite Element Analysis

Benjamin Anthony[1] · Nathan Fripp[1] · Tianchen Wei[1] · Benjamin A. Begley[1] · Victoria M. Miller[1]

Accepted: 9 July 2024 / Published online: 22 July 2024

Abstract

Material properties have often only been considered in analyses of laser sheet metal forming in the manner that they contribute to the bulk operating-temperature mechanical properties of the metal. In fact, many properties critical to laser sheet metal forming—such as yield strength and coefficient of thermal expansion—are dependent on temperature and crystallographic orientation, and thus vary considerably during the forming process, complicating bend angle prediction. The effects of temperature and orientation dependence of these properties—and especially the profile of the temperature-property curve—are investigated using a thermomechanical model in the Abaqus finite element modeling software. The models indicate that, while bending is possible even when properties are assumed to be constant with temperature, sharp transitions in temperature-dependent properties can greatly enhance bending, providing a screening metric for the selection of materials for laser sheet metal forming.

Keywords Laser forming · Sheet metal forming · Finite element analysis · Abaqus

Introduction

The role of material properties in laser sheet metal forming has often been underconsidered. This is likely one of the contributing factors to the relatively poor performance of models attempting to predict resultant bend angles [1]. Further research into the complex interplay of temperature-dependent material properties and the evolving stress states within the material are necessary. The temperature gradient mechanism (TGM) of laser bending is the most widely modeled. In this mechanism, only a fraction of the sheet thickness is meaningfully heated, resulting in a steep thermal gradient

✉ Tianchen Wei
tianchen.wei@ufl.edu

[1] Department of Materials Science and Engineering, University of Florida, Gainesville, Florida 32611, USA

through the thickness. The heated surface region thermally expands, initially resulting in a bend away from the laser beam (counterbending). At the same time, the thermal expansion of the heated region is constrained by the surrounding material. Within the heated region the resistance to plastic deformation is also typically reduced due to thermal softening of the material. The combination of thermal softening and constraint results in compressive plasticity in the heated region. Upon cooling, the plasticity is not reversed and the compressive deformation results in an upward bend [2, 3].

As described, there are many temperature-dependent material parameters that are crucial to the TGM. The thermophysical properties — thermal conductivity, surface absorptivity to the laser wavelength, specific heat capacity, density, coefficient of thermal expansion (CTE) — all directly impact the geometry of the heated zone. The mechanical properties of the material—modulus and yield strength—determine the extent of deformation that occurs. Shichun et al. experimentally demonstrated that increasing the ratio of CTE to the density multiplied by the specific heat leads to more bending [4]. Many of these properties are also anisotropic, depending on crystallographic direction.

The first analytical model derived for the TGM was derived by Vollertsen [5]. This two-layer model included the CTE, density, and specific heat capacity, but no other material parameters. This model was later extended by Yau et al. to incorporate counterbending, resulting in consideration of the yield strength and elastic modulus [6]. However, these initial formulations did not account for temperature dependence or anisotropy. Later, Shen et al. derived an analytical model that incorporates thermal softening of the heated region to a constant reduced value and explicitly describes the extent of the plastic region [7]. McBride et al. developed a simple analytical thermal model that takes into account the temperature dependent yield stress, but not the temperature dependent thermal expansion [8]. Chakraborty et al. found that the mechanical properties of the sheet impacted the final bend angle; adding prior compressive or tensile stresses increased and decreased, respectively, the final bend angle as compared to an unstressed sheet [9]. Work by Mulay et al. on a more accurate analytical model has demonstrated success by utilizing the thermally dependent thermal expansion, but neglects temperature effects on yield stress [10].

Finite element (FE) models of laser forming have developed in parallel with the analytical models described above. The parameterization and numerical implementation of an FE model make the incorporation of temperature-dependent material property profiles straightforward. Consequently, the material properties implemented are typically more realistic [11–16], e.g., Yilbas et al. implemented temperature-dependent Young's modulus, thermal expansion coefficient, and thermal conductivity using fixed values within binned temperature ranges [14]. Guan et al. used FE methods to demonstrate the role of different magnitudes of Young's modulus, yield strength, thermal expansion coefficient, specific heat, and thermal conductivity on the resultant bend angle [17]. Ultimately, the present work is inspired by this study. While Guan imposed constant values for the studied variables, herein the shapes of the material property profiles are investigated.

The primary objective of this work is to determine the role of the shape of the temperature-dependent material property profiles on the resultant bend angle. The secondary objective is to demonstrate the potential magnitude of the role of material

anisotropy. While the focus of this study is on the TGM, the approach taken herein is equally relevant to the buckling and upsetting laser forming mechanisms.

Methodology

In this work, Abaqus 2021 finite element analysis software was used to evaluate how changes in thermomechanical properties modified the resulting bend angle during laser forming. Abaqus is commonly used in industry to simulate sheet metal forming operations, and can be parameterized to account for thermally induced deformation such as by thermal expansion.

The sample geometry considered is shown in Fig. 1a, consisting of a uniform sheet with dimensions of 30x10x0.5 mm. A variable mesh size was used across the specimen,

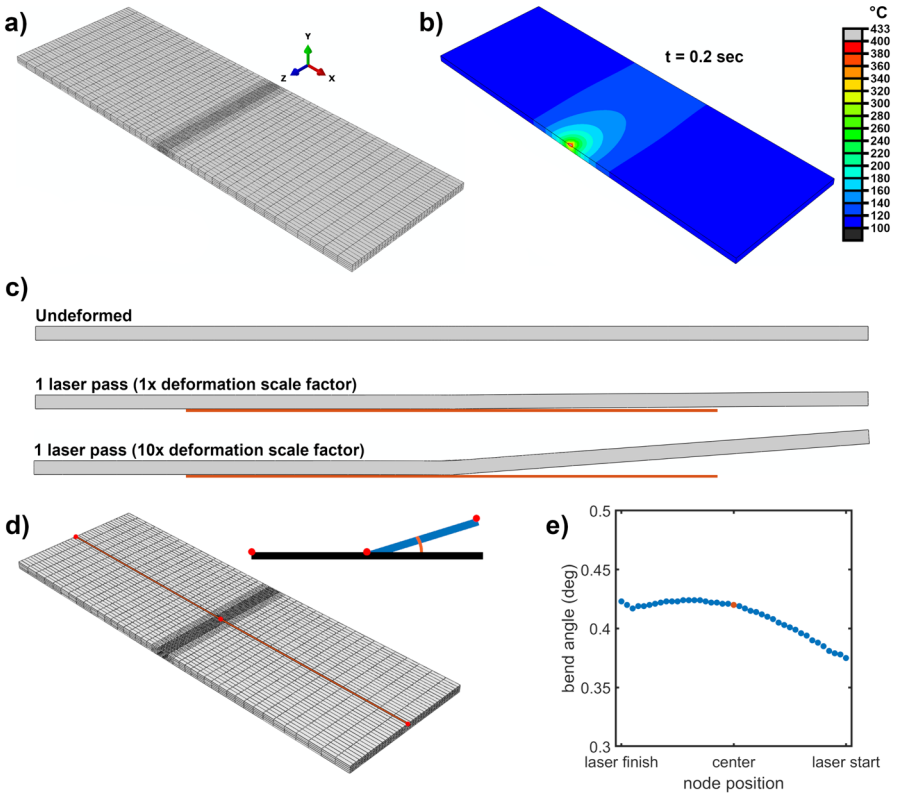

Fig. 1 *a*) Meshed FEA model (9920 elements) used to emulate Al sheet measuring 30x10x0.5 mm. The laser path is along Z on the center of the top surface. *b*) Temperature at the end of the laser heating step, prior to a 0.2 s cooldown step. *c*) Profile view (XY plane) of the undeformed specimen (top) and after bending (middle). A 10x deformation scale factor (bottom) and guide lines (orange) are provided to ease visualization due to the small bend angle. *d*) Three node method used to calculate the bend angle of a single line along the sample using the top surface, with schematic side-view. *e*) Bend angle measurements taken along parallel lines across the sample width, with the line in *d* shown in orange

Table 1 Physical properties of AA 3003 used to parameterize the simulation [18]

Property	Value	Unit
Density	2730	kg/m^3
Elastic Modulus	68.9	GPa
Poisson's Ratio	0.33	
Thermal Conductivity	163	W/m-K
Specific Heat	893	J/kg-K
Absorption	12	%

While laser absorption is not an explicitly defined material parameter in Abaqus, this value was used in the DFLUX subroutine to modulate the heat flux from the laser

with the center of the specimen's length (where bending would be localized) having a finer mesh size. A total of 9920 elements were used. The sheet was generally parameterized to emulate AA 3003 aluminium alloy in the H14 temper. The values for thermal and mechanical properties used are given in Tables 1 and 2, including temperature-dependent values for thermal expansion and yield strength. Particular parameters were then modified to interrogate the resultant bending behavior, as outlined below.

The laser was represented by a moving circular surface heat source with a diameter of 0.5 mm. The laser being emulated was a 70 W pulsed fiber laser with a wavelength of 1064 nm and pulse rate of 20 kHz. In order to simplify the model and lower computational cost, the simulated laser interaction was assumed to behave as a uniformly-distributed continuous-wave heat flux of 1071 mW/mm^2, which was then multiplied by an absorption coefficient of 0.12 to achieve a final laser heat flux of 128.5 mW/mm^2.

A DFLUX subroutine was used to raster the laser across the width of the specimen at its center in a straight line, as shown in Fig. 1b. The raster velocity was 50 mm/s, for a pass duration of 0.2 seconds. Each simulation consisted of a single laser pass, followed by a "cool down" step of the same duration (0.2 s) with no active heat source to allow the heat to diffuse. This was necessary to reduce uneven thermal expansion through the thickness of the sheet, enabling better measurements of the final bend angle due to plastic deformation. For the purposes of this work, heat loss due to convection

Table 2 Temperature-dependent mechanical properties of AA 3003-H14 used to initially parameterize the simulation [18]

Temp. (°C)	Yield Stress (MPa)	CTE (10^{-6}/K)
25	145	
100	130	23.2
200	62	24.1
300	17	25.1
400	12	

Yield stress and CTE between the listed temperatures was determined *via* linear interpolation. Above the maximum temperature listed for each value, the stress or coefficient at the maximum temperature is used

or conduction to the surroundings were ignored for computational efficiency and to capture variances in bending due to internal heat diffusion rather than heat loss to the environment. Additionally, the initial temperature of the specimen was set to 100°C to ensure that the induced thermal gradient would capture the entire thermal softening effect present in the AA 3003-H14 yield profile.

An example of the sheet deformation is shown in Fig. 1c. After bending was completed, the bend angle was measured using the angle measurement tool within Abaqus *via* the three node method, using the end points and center point as shown in Fig. 1d. The angle was measured on the top surface, and a separate measurement was taken for each set of three nodes across the width of the specimen to capture changes in variance between test conditions. An example of this variance across the specimen is shown in Fig. 1e.

The impact of temperature-dependent yield behavior was assessed by varying the trends in yield stress as a function of temperature. The initial yield stress as a function of temperature for AA 3003-H14 is given in Table 2 as well as shown in Fig. 2.

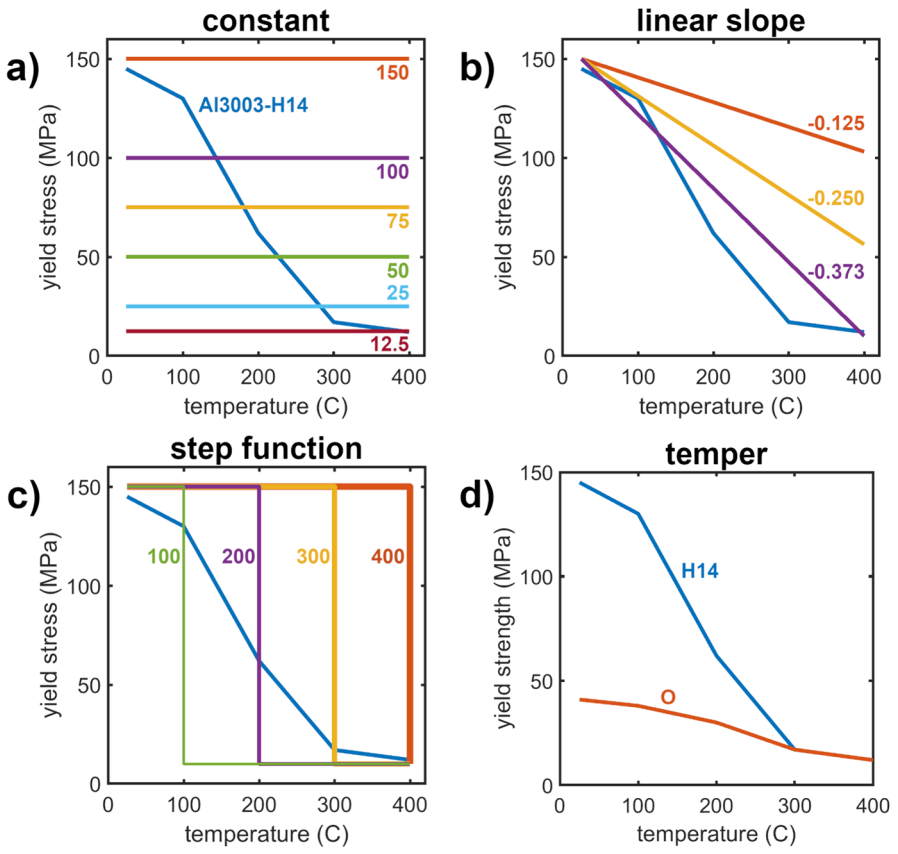

Fig. 2 Profiles of yield stress as a function of temperature used. The AA 3003-H14 yield behavior was modified to produce *a*) constant yield stresses, *b*) linear slopes, and *c*) step functions. *d*) Material temper was considered using the "O" (annealed) condition [18]

Constant yield stresses were considered from across the range of values this alloy can exhibit at various temperatures, as shown in Fig. 2a. A linear approximation of the temperature softening curve was also considered as well as two additional linear slopes, as shown in Fig. 2b. To examine how sudden changes in yield point modify the bend behavior, step functions with varying transition temperatures were used as shown in Fig. 2c. Additionally, the role of temper was examined by comparing yield behavior of the H14 temper to that of the O temper (Fig. 2d) [18].

The role of the CTE and its temperature dependence were similarly assessed. Constant values were taken from those present in AA 3003 across the considered temperature range (Fig. 3a). As the CTE of this material is close to linear, multiples of the slope (>1x, <1x, and -1x) were examined as seen in Fig. 3b-d. The sign of the CTE, such as for a negative thermal expansion coefficient, was also considered (Fig. 6a). Sudden changes in the CTE were examined using step functions with varied temperatures, as well as a variation in the difference between the pre- and post-step coefficients (Fig. 3e). Additionally, the orientation-dependence of the CTE (Fig. 3f) was examined by taking the initial values as expansion in the ⟨001⟩ directions and multiplying by factors of $\sqrt{2}$ for ⟨011⟩ and $\sqrt{3}$ for ⟨111⟩.

Results

After a single laser pass of the given parameters and subsequent heat diffusion step, the thermal and mechanical behavior of AA 3003-H14 were found to produce a median bend of 0.42°, which will be used as a baseline for comparison. The maximum tem-

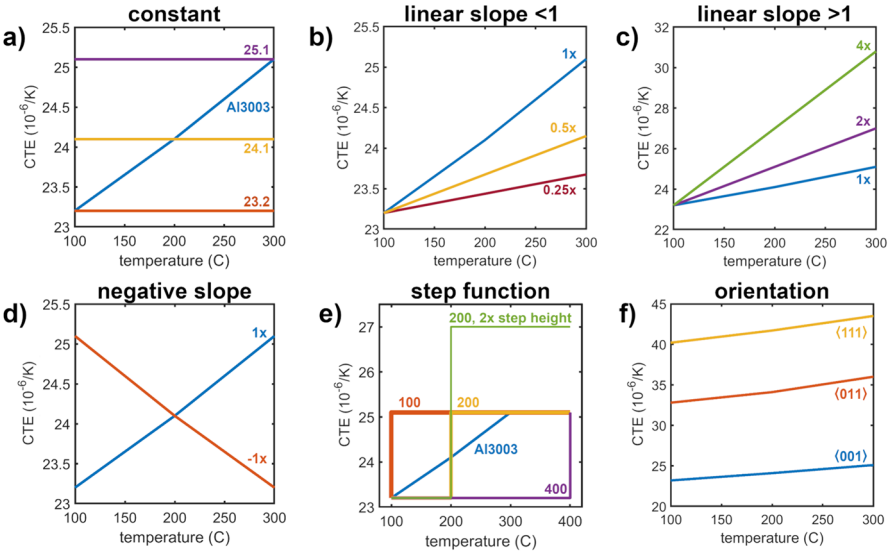

Fig. 3 Profiles of the coefficient of thermal expansion as a function of temperature used. The AA 3003 behavior was modified to produce *a*) constant CTEs, *b*) linear slopes less than 1x, *c*) linear slopes greater than 1x, *d*) negative slope, *e*) step functions, and *f*) crystallographic orientation-dependent behavior

perature at the end of the heating step was 433.4°C, and the maximum at the end of the heat diffusion step was 127.6°C.

Temperature-Dependent Yield Stress

The constant yield stress profiles (Fig. 2a) produced a wide range of resultant bend angles, as shown in Fig. 4a. Even with the value held constant, bending was still able to occur. As the yield point increases, the bend angle produced by a single laser pass is seen to increase to a maximum around 50 MPa before decreasing rapidly. While the highest fixed yield point considered of 150 MPa produced only a small amount of bending (about 0.01°), the thermally-induced stresses were still capable of inducing plastic strain in the material. Notably, all constant yield point values were found to induce less bend than the baseline AA 3003 behavior.

When the yield profile was changed to be linear (Fig. 2b), the resultant bend angles, shown in Fig. 4b, significantly decreased in a similar fashion to the constant yield

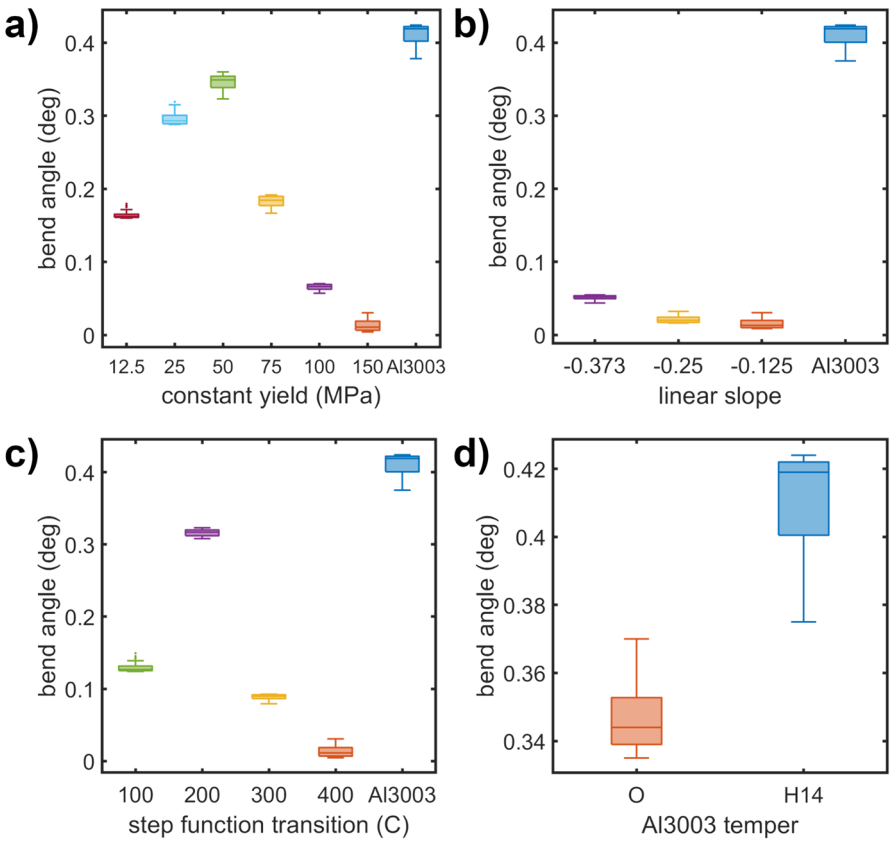

Fig. 4 Bend angles produced by a single laser pass after modifying the yield profile to be *a*) constant, *b*) linear slopes, *c*) step functions, and *d*) the "O" temper condition

stresses of 100 and 150 MPa. Even when the slope was a linear approximation of the actual AA 3003 profile, only around 1/8th of the amount of bending occurred. This significant change in behavior appears to indicate that sharp drops in the yield stress across a given temperature range are important contributors to bending during laser forming.

This contribution was further examined by considering step functions (Fig. 2c), wherein the yield would start at 150 MPa and then, upon exceeding the transition temperature, drop to 12.5 MPa. The bend angles produced from varying transition temperatures are shown in Fig. 4c. Similar to the constant yield point cases, the trend increases to a maximum around a transition temperature of 200°C before rapidly declining to values expected from maintaining a constant 150 MPa yield point. This maximum approaches the angle seen at a constant 50 MPa and approximately doubles that of the constant 12.5 MPa case, while significantly exceeding the degree of bending seen in the constant 150 MPa case or any of the linear profiles. The presence of a sudden drop in yield stress greatly increased the resultant bend compared to either of its constituent constants, further supporting this yield behavior as an important contributor to bending; however, even the maximum value obtained via a step function profile was still less than that of the actual AA 3003.

To further investigate these trends in behavior, an additional yield profile was considered to emulate AA 3003 in the O tempered (fully annealed) state. A comparison of the temperature-dependent yield point between the two tempers is shown in Fig. 2d. As the O temper yields at a far lower stresses than H14 until 300°C and the overall decline in the profile is more shallow, the O temper material was expected to behave more similarly to a constant yield point and thus bend significantly less. The resultant bends are shown in Fig. 4d. While AA 3003-O did achieve a lower bend angle than AA 3003-H14, the extent of bending was similar to that of the constant 50 MPa yield stress or the step function with a transition at 200°C, despite remaining below 40 MPa for the temperature range considered and without a sharp drop in yield point. Comparing this to the behavior of other profiles, the amount of bending achieved appears to not just depend on the absolute value of the yield point, but also on the relative differences across the yield profile.

Temperature-Dependent CTE

As the CTE of AA 3003 increases nearly linearly within the considered temperature range, the values at 100, 200, and 300°C were held constant (Fig. 3a) for the sake of comparison. The resulting bend angles are shown in Fig. 5a, and illustrate a similarly linear increase that corresponds with increases in CTE. As with the yield stress behavior, the angles produced by these constant thermal expansion coefficients were non-zero, indicating that bending is possible; however, all are still lower than the actual AA 3003 values.

To interrogate how the steepness of the slope in the temperature-dependence of CTE affects the resultant bend, additional slopes were tested as multiples of the base AA 3003 values, as shown in Fig. 3b-d. The bend angles produced by these varied slopes are presented in Fig. 5b and c, and indicate that the resultant bend is directly

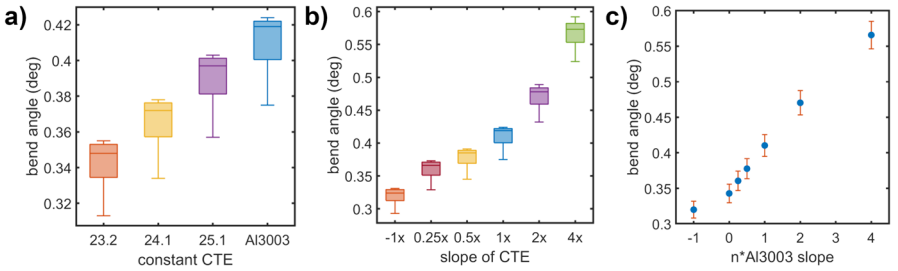

Fig. 5 Bend angles produced by a single laser pass after modifying the CTE profile to be *a*) constant and *b*) linear slopes. *c*) Mean bend angles with one standard deviation error bars for *n* multiples of the AA 3003 slope. For n = 0, the constant 23.2 10^{-6}/K value was used

correlated to amount of change in CTE with temperature. Multiples greater than one induced more bending in the specimen, while fractions of the original slope induced a reduced amount of bend. Notably, even when the slope was inverted (producing less expansion as temperature increases), bending still occurred but was diminished, to the point of even being below those of the lowest constant CTE case. The instance of a negative thermal expansion coefficient was subsequently considered with results shown in Figs. 6b and c. When the material contracts as temperature increases, the resultant bend is equal in terms absolute value but opposite in terms of sign, with the specimen bending downwards instead of upwards.

The behavior of discontinuities in the CTE profile were examined using step functions with transitions at 100, 200, and 400°C as shown in Fig. 3e, with two different step heights considered for 200°C. Similar to the step functions considered for yield behavior, the resultant bends (Fig. 7a and b) increase as the transition temperature increases up to 200°C before trending downward, with the 200°C transition point achieving more bending than the AA 3003 behavior. When the step height was doubled, the resultant bend increased further, indicating that the severity of the discontinuity similarly has a direct effect on the amount of bending achieved.

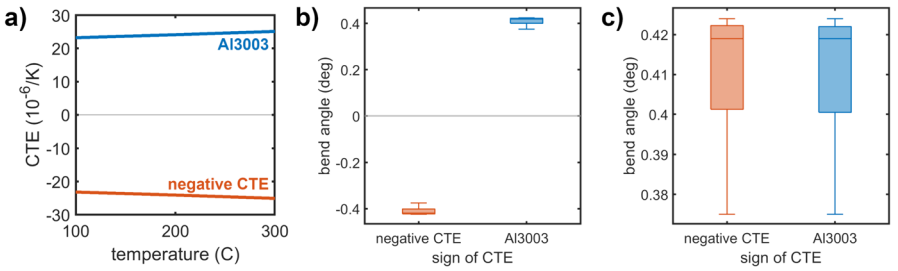

Fig. 6 *a*) Profile of a negative temperature-dependent CTE, or thermal compression. By changing the sign of the CTE profile, *b*) the actual bend angle becomes negative (downward bending), while *c*) the absolute value of the bend angle is found to be equal to that of the initial behavior

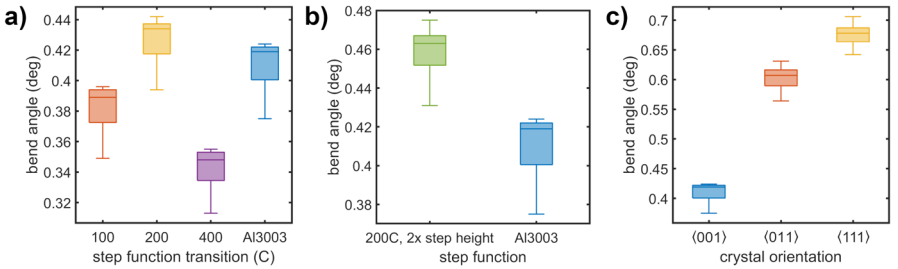

Fig. 7 Bend angles produced by a single laser pass after modifying the CTE profile to be step functions of *a*) varying transition temperature and *b*) increased step height, as well as *c*) varied crystallographic orientation

Orientation-dependent CTE

Due to the different relationships between the unit cell lengths of various crystallographic directions and the lattice parameter, changes in orientation relative to the sample X direction were considered. The AA 3003 CTE values were assumed to be that of the ⟨001⟩ direction, with the corresponding ⟨011⟩ and ⟨111⟩ coefficients shown in Fig. 3f and bend angles shown in Fig. 7c. The yield profile was kept constant throughout. As the expansion in these directions is greater than that for the ⟨001⟩, the resulting bends are significantly increased. This behavior indicates that bending behavior is likely strongly dependent upon crystallography, grain size, and crystallographic texture.

Discussion

Modifying the shapes and intensities of the yield and CTE profiles was found to have a direct impact on the material's resultant bend angle, providing a number of insights into elastic and plastic mechanical properties that can aid or hinder the ability of a material to be bent *via* laser forming. The only instances in which no plastic deformation occurred were when there was no thermal expansion at all, or when the yield point was too high to be achieved with the given laser parameters. For the latter case, this does not indicate that that materials with a high yield strength cannot be bent, but rather that the laser power or raster speed would need to be modulated differently (or a surface coating applied to boost absorptivity) in order to get a heating profile suitable for producing higher stresses. Essentially, as long as a material undergoes thermal expansion, there will be a set of laser parameters that results in bending.

The analytical model described in McBride et al. modeled the development of plastic strains in the TGM using two discrete stages: a stage during heating in which the expanded region plastically deforms due to rigid constraint of the cooler surrounding material, and then a stage during cooling in which the previously expanded region contracts and further resultant stresses cause additional plastic deformation [8]. By considering the effect of temperature-dependent yield and CTE profiles separately in these stages, an explanation for the seemingly counter-intuitive bending behaviour

seen at the lower end of the constant yield point tests (Fig. 4a) begins to emerge. During the initial heating and expansion stage, the low yield point results in greater amounts of internal compressive strain. However, as the heated region cools and contracts, it is similarly easy for the yield point in the compressed regions to be overcome and expand, negating the deformation that contributes to bending. This can also be seen in the reduction in bending for AA 3003-O temper (Fig. 4d) as the decreased yield point at lower temperatures enables more plastic expansion of the initially-compressed regions upon cooling. The local maximum in bending at the 200°C transition step function may also be considered in terms of these stages. The heating/expansion stage exceeds the transition temperature and thus deforms readily due to the constraint of the surrounding cooler, and thus significantly harder, material which in turn produces a moderate bend.

Thermal expansion plays a powerful role in generating the stresses necessary to achieve plastic deformation during laser forming, with every aspect of the temperature-dependent CTE profile having a noticeable impact on the final bend angle. When the thermal expansion coefficient was held constant, the exact value used had a linear relationship with the bend; when the coefficient increased linearly with temperature, the final bend had a similar linear relationship with the slope of the temperature-dependence. If a discontinuity was present, both the temperature and severity of the discontinuity would modify the amount of bending achieved.

Considering all of these aspects together provides an initial basis to screen the relative amount of bending possible with a single laser pass, just from thermal expansion data. Materials that have higher linear thermal expansion coefficients and with greater increases in CTE over the temperature range induced by the laser should, for an equivalent yield stress profile, produce noticeably more bending. Similarly, materials with intense discontinuities or other jumps in their thermal expansion behavior should have particularly good bending behavior.

The effect of crystallographic orientation on the thermal expansion coefficient—and thus in turn the bend angle—is of particular note. Generally, past studies attempting to model bending behavior either computationally or analytically have tended to assume the material is uniform and isotropic [1]. This assumption rarely holds for sheet metals, as the rolling process can impart significant crystallographic texture. In demonstrating that the crystallographic orientation of a single crystal has a significant effect on the total extent of bending, it holds that a non-uniform distribution of polycrystal orientations will also have such an effect. Where mechanical properties are concerned, the response of a polycrystalline system can generally be treated as a weighted average of the single crystal responses over the orientation distribution function that makes up the polycrystal [19–21]. Due to the symmetry of the FCC crystal lattice, the ⟨001⟩ and ⟨111⟩ orientations are the extremes of the crystalllographic orientation dependence; regardless of the polycrystal orientation distribution, the bend angle will lie between these two bend angle values if no other feature is changed. Given that the orientation distribution can have a significant effect even for a highly symmetric crystal system, this indicates that the specific crystallography of the material may contribute directly to bending behavior as different unit cells with lower symmetry may have more drastic orientation effects.

Even for cubic materials, the initial grain size relative to the laser spot size will also serve as an important factor as fine-grained material will effectively use a combination of the CTE for multiple differently oriented grains, while coarse-grained material will be much more sensitive to the orientation of the specific grain(s) hit by the laser. As grain size is controlled by the production method and any subsequent deformation processes or heat treatments, every step in the production of the part will play a role in its susceptibility to bending. Similarly, prior deformation (such as during sheet rolling) can lead to crystallographic texture, in which certain crystal orientations are more prevalent throughout the microstructure, which in turn will modify the degree to which a part will bend during a given laser forming operation. These previously unexamined microstructural factors may play a key role in explaining the large variation between reported bend angles in previous studies into laser forming.

The scenario considered here is not perfectly identical with reality, and experimental results into orientation effects may not be as drastic as seen here. In the current work, the orientation dependence was investigated solely by modifying the CTE based off of geometric considerations. In essence, the sheet was considered a single crystal for the purposes of thermal expansion, but the yielding behavior remained identical across the different orientations. In reality, a given sheet of material would be a polycrystal containing grains of many different orientations. Not only would the thermal expansion depend upon the orientation of a given grain, but the resolved shear stresses that result in yielding would also similarly be dependent upon orientation. As these particular yield effects are not captured by the current model, a more thorough study into the role of orientation and crystal plasticity on laser forming is necessary to better understand the extent to which they contribute to bend angle.

Using the temperature-dependent thermal expansion behavior determined in this work as a guide, it is possible to make some estimations of how favorable bending is in different materials, all else being equal. In this regard, aluminum is actually an exceptionally good choice of material for bending applications as the CTE for pure Al ranges from 23.5 to 26.5 10^{-6}/K between 300 and 500 K [22], both a high baseline value and sizeable increase with temperature (Table 3). Other ductile FCC metals such

Table 3 Coefficients of linear thermal expansion for various pure metals across ranges of 300 to 500 K

Material	CTE (10^{-6}/K)	Δ CTE	Reference
Aluminum	23.5-26.5	3.0	[22]
Copper	16.5-18.0	1.5	[22]
Gold	14.0-15.0	1.0	[22]
Tungsten	4.3-4.5	0.2	[23]
Molybdenum	5.1-5.5	0.4	[24]
Nickel	12.5-15	2.5	[22]
Iron	11.5-14	2.5	[22]
Lead	29.3	–	[18]
Zinc	31.0-36.5	5.5	[25]
Cadmium	31.3	–	[18]

Materials presented with a single value are at 300 K

as copper and gold would in turn bend less than Al due to having both a lower initial CTE (16.5 and 14.0 10^{-6}/K, respectively) and smaller increase over this temperature range [22]. Refractory metals such as tungsten and molybdenum are expected to have very low amounts of bending per laser pass, as their thermal expansion coefficients are only around 20% of that of Al and increase very little with temperature [23, 24].

Nickel and iron have an initial value of around 50% that of aluminum but see a similar amount of increase over this temperature range, making them favorable candidates for bending. Notably, both of these metals also have anomalous expansion behavior that results in increased slopes at temperatures just above 500 K which would likely result in even greater amounts of bending per pass than can be predicted here [22]. These same anomalous properties are utilized in the Fe-Ni alloy Invar to produce a very low thermal expansion at room temperature, around 1 10^{-6}/K [26]. Counterintuitively, this behavior actually makes Invar predicted to be exceptionally good for bending as the CTE rapidly increases to more typical values between 200 and 300°C [27], resulting in a situation akin to the step function profiles shown in this work and likely producing substantial amounts of bending per laser pass. On the other hand, Ti-based ALLVAR has a CTE of -30 10^{-6}/K at room temperature [28]. ALLVAR is predicted to exhibit downward bending for identical laser parameters that develop upward bending in other metals.

While it may be of interest to experiment with materials that have a higher starting CTE than Al, three of the most readily available metals that fit this criteria are lead, zinc, and cadmium with values of around 29, 31, and 31 10^{-6}/K, respectively [18, 25]. As this is about 25% greater than aluminum, there should be a commensurate increase in the bend per pass; however, as these metals pose significant health hazards when heated to the temperatures involved in laser forming, increased safety precautions would be necessary. Additionally, in making any predictions here based on the comparative thermal expansion coefficients, everything else is assumed to be equal including the heat input from the laser and the yield behavior. As these would vary greatly between materials under the same laser power and raster parameters, the CTE differences alone will not be enough to accurately predict the actual amount of bending achieved in a single pass, but may give insights into some fundamental differences in behavior across various metals.

Conclusions

Abaqus finite element modeling was used to determine the roles of the yield stress and thermal expansion in laser forming using AA 3003 aluminum alloy. By modifying the temperature-dependent profiles of these two parameters, the following was determined:

- Bending was able to occur even when the yield stress or thermal expansion coefficient was held constant.
- Both constant yield stresses and step functions were found to have a trend with a maximum bend angle at an intermediate value.

- A linear approximation of the AA 3003 yield profile resulted in greatly diminished bending, indicating sharp transitions in the yield point contribute heavily to bending behavior.
- The lower yield stresses of the O temper AA 3003 resulted in a smaller bend angle than the harder H14 temper.
- Increasing the value of a constant CTE or the slope of the CTE with temperature both increase the bend angle.
- Step function profiles for CTE were found to depend both on the step transition temperature and the height of the step.
- The crystallographic orientation of the material strongly impacts the amount of bending achieved, with the ⟨111⟩ direction producing the greatest bend angle.

From these findings, the combination of temperature-dependent yield stress and CTE profiles may be able to serve as a preliminary screening tool for candidate materials for laser forming, or to evaluate a given material's inherent susceptibility to bending via this method.

Acknowledgements The authors would like to thank Professor Matthew Begley from the University of California Santa Barbara for insightful discussions that led to this work.

Author Contributions Study conception and design were contributed to by B.A., B.B., and V.M. Modeling procedure, data collection, and analysis were performed by B.A. The first draft of the manuscript was written by B.A., N.F., T. W., and B.B. All authors commented on and revised the manuscript, and all authors read and approved the final manuscript.

Funding This work was funded by the DARPA NOM4D program, Contract Number HR001122C0044. T. Wei was additionally supported by the Nuclear Regulatory Commission award number 31310021M0025.

Data Availability Data can be made available upon reasonable request.

Declarations

Competing interest The authors declare no competing interests.

References

1. Shen, H., Vollertsen, F.: Modelling of laser forming – An review. Comput. Mater Sci. **46**(4), 834–840 (2009). https://doi.org/10.1016/j.commatsci.2009.04.022. https://linkinghub.elsevier.com/retrieve/pii/S0927025609001888
2. Geiger, M., Vollertsen, F.: The Mechanisms of Laser Forming. CIRP Ann. **42**(1), 301–304 (1993). https://doi.org/10.1016/S0007-8506(07)62448-2
3. Magee, J., Watkins, K.G., Steen, W.M.: Advances in laser forming. J. Laser Appl. **10**(6), 235–246 (1998). https://doi.org/10.2351/1.521859. http://lia.scitation.org/doi/10.2351/1.521859
4. Shichun, W., Jinsong, Z.: An experimental study of laser bending for sheet metals. J. Mater. Process. Technol. **110**(2), 160–163 (2001). https://doi.org/10.1016/S0924-0136(00)00860-8. https://linkinghub.elsevier.com/retrieve/pii/S0924013600008608
5. Vollertsen, F.: An analytical model for laser bending. Lasers in Engineering **2**, 261–276 (1994)
6. YAU, C. L.: A New Analytical Model for Laser Bending, Laser Assisted Net Shape Engineering 2, Proceedings of the LANE' **97**, 357–366 Publisher: Meisenbach Bamberg. https://doi.org/https://ci.nii.ac.jp/naid/10005326784/

7. Shen, H., Yao, Z., Shi, Y., Hu, J.: An analytical formula for estimating the bending angle by laser forming. Proc. Inst. Mech. Eng. C J. Mech. Eng. Sci. **220**(2), 243–247 (2006). https://doi.org/10.1243/095440606X79721. http://journals.sagepub.com/doi/10.1243/095440606X79721
8. McBride, R., Bardin, F., Gross, M., Hand, D.P., Jones, J.D.C., Moore, A.J.: Modelling and calibration of bending strains for iterative laser forming. J. Phys. D Appl. Phys. **38**(22), 4027–4036 (2005). https://doi.org/10.1088/0022-3727/38/22/005
9. Chakraborty, S.S., More, H., Racherla, V., Nath, A.K.: Modification of bent angle of mechanically formed stainless steel sheets by laser forming. J. Mater. Process. Technol. **222**, 128–141 (2015). https://doi.org/10.1016/j.jmatprotec.2015.02.044. https://linkinghub.elsevier.com/retrieve/pii/S0924013615001016
10. Mulay, S., Paliwal, V., Babu, N.R.: Analytical approach to predict the bend angle of sheet formed by multiple laser scans. Procedia CIRP **99**, 272–277 (2021). https://doi.org/10.1016/j.procir.2021.03.040
11. Bao, J., Yao, Y.L.: Analysis and Prediction of Edge Effects in Laser Bending, Journal of Manufacturing Science and Engineering 123(1), 53–61. https://doi.org/10/ffw4j2. https://asmedigitalcollection.asme.org/manufacturingscience/article/123/1/53/458886/Analysis-and-Prediction-of-Edge-Effects-in-Laser
12. Loeschner, U., Exner, H.: FEM calculations on laser bending of silicon with a moving laser source. In: MEMS, MOEMS, and Micromachining, vol. 5455, SPIE, pp 407–414 (2004). https://doi.org/10.1117/12.544814. https://www.spiedigitallibrary.org/conference-proceedings-of-spie/5455/0000/FEM-calculations-on-laser-bending-of-silicon-with-a-moving/10.1117/12.544814.full
13. Zhang, X.R., Xu, X.: Finite Element Analysis of Pulsed Laser Bending: The Effect of Melting and Solidification. J. Appl. Mech. **71**(3), 321–326 (2004). https://doi.org/10.1115/1.1753268
14. Yilbas, B.S., Arif, A.F.M., Abdul Aleem, B.J.: Laser bending of AISI 304 steel sheets: Thermal stress analysis, Optics & Laser Technology **44**(2), 303–309 (2012) . https://doi.org/10.1016/j.optlastec.2011.06.021. https://www.sciencedirect.com/science/article/pii/S0030399211001812
15. Xu, L., Li, W., Wang, X., Wan, M., Jiang, M.: Plastic deformation behavior in laser bending of elastic pre-loaded metal plate. Int. J. Adv. Manuf. Technol. **90**(9), 3397–3406 (2017). https://doi.org/10.1007/s00170-016-9643-8. https://doi.org/10.1007/s00170-016-9643-8
16. Shi, Y., Guo, Y., Wang, X., Sun, R., Li, X.: Laser bending angle and surface quality with preload at low heating temperature. Optics & Laser Technology **136**, 106755 (2021). https://doi.org/10.1016/j.optlastec.2020.106755. https://linkinghub.elsevier.com/retrieve/pii/S0030399220313888
17. Guan, Y., Sun, S., Zhao, G., Luan, Y.: Influence of material properties on the laser-forming process of sheet metals. J. Mater. Process. Technol. **167**(1), 124–131 (2005). https://doi.org/10.1016/j.jmatprotec.2004.10.003
18. Metals Handbook Vol. 2 - Properties and Selection: Nonferrous Alloys and Pure Metals, 9th edn, (1979)
19. Bunge, H.J.: Texture Analysis in Materials Science: Mathematical Methods, Butterworths, (1982), google-Books-ID: ODdRAAAAMAAJ
20. Kocks, U.F., Tomé, C.N., Wenk, H.-R.: Texture and Anisotropy: Preferred Orientations in Polycrystals and their Effect on Materials Properties, Cambridge University Press, (1998)
21. Man, C.-S.: Crystallographic Texture and Group Representations. J. Elast. **149**(1), 3–445 (2022). https://doi.org/10.1007/s10659-022-09882-8
22. Nix, F.C., MacNair, D.: The thermal expansion of pure metals: Copper, gold, aluminum, nickel, and iron. Phys. Rev. **60**(8), 597–605 (1941). https://doi.org/10.1103/PhysRev.60.597
23. Hidnert, P., Sweeney, W.: Scientific Papers of the Bureau of Standards: Thermal Expansion of Tungsten, Scientific Papers of the Bureau of Standards **20**, 483–487 (1925). https://nvlpubs.nist.gov/nistpubs/ScientificPapers/nbsscientificpaper515vol20p483_A2b.pdf
24. Hidnert, P., Gero, W.B.: Thermal Expansion of Molybdenum. Scientific Papers of the Bureau of Standards **19**, 429–444 (1924). https://doi.org/10.6028/nbsscipaper.171
25. Austin, J.B.: A vacuum apparatus for measuring thermal expansion at elevated temperatures, with measurements on platinum, gold, magnesium and zinc. J. Appl. Phys. **3**(5), 240–267 (1932). https://doi.org/10.1063/1.1745131
26. Shiga, M.: Invar alloys. Curr. Opin. Solid State Mater. Sci. **1**(3), 340–348 (1996). https://doi.org/10.1016/S1359-0286(96)80023-4

27. Matsui, M., Chikazumi, S.: Analysis of Anomalous Thermal Expansion Coefficient of Fe–Ni Invar Alloys. J. Phys. Soc. Jpn. **45**(2), 458–465 (1978). https://doi.org/10.1143/JPSJ.45.458
28. Monroe, J.A., East, M., Hull, T.B.: ALLVAR alloy athermalization: a novel and cost-effective alternative for small to moderate sized space telescopes. In: Hallibert, P., Hull, T.B., Kim, D., Keller, F. (eds.), Astronomical Optics: Design, Manufacture, and Test of Space and Ground Systems III, SPIE, San Diego, United States, p. 13 (2021). https://doi.org/10.1117/12.2594816. https://www.spiedigitallibrary.org/conference-proceedings-of-spie/11820/2594816/ALLVAR-alloy-athermalization--a-novel-and-cost-effective-alternative/10.1117/12.2594816.full